

## Article

# Thermal Transformation of Natural Schwertmannite in the Presence of Chromium

Carlos Lázaro <sup>1</sup>, Juan Antelo <sup>2,\*</sup> , Ivan Carabante <sup>3</sup>, Alba Otero-Fariña <sup>4</sup> , Pedro V. Verdes <sup>5</sup>,  
Bruno Dacunha-Marinho <sup>6</sup>  and Sarah Fiol <sup>1</sup> 

- <sup>1</sup> CRETUS, Department of Physical Chemistry, Universidade de Santiago de Compostela, 15782 Santiago de Compostela, Spain; carlos.lazaro@rai.usc.es (C.L.); sarah.fiol@usc.es (S.F.)
- <sup>2</sup> CRETUS, Department of Soil Science and Agricultural Chemistry, Universidade de Santiago de Compostela, 15782 Santiago de Compostela, Spain
- <sup>3</sup> Waste Science and Technology, Department of Civil, Mining & Environmental Engineering, Luleå University of Technology, SE-97187 Luleå, Sweden; ivan.carabante@ltu.se
- <sup>4</sup> School of Earth and Environment, University of Leeds, Leeds LS2 9JT, UK; a.oteroarina@leeds.ac.uk
- <sup>5</sup> Soft Matter and Molecular Biophysics Group, Department of Applied Physics, Universidade de Santiago de Compostela, 15782 Santiago de Compostela, Spain; pedro.vazquez@usc.es
- <sup>6</sup> Unidade de Raios X, RIAIDT, Universidade de Santiago de Compostela, 15782 Santiago de Compostela, Spain; bruno.dacuna@usc.es
- \* Correspondence: juan.antelo@usc.es; Tel.: +34-881-816042

**Abstract:** Schwertmannite is a metastable mineral playing a crucial role in the immobilization of metal(oid)s in acid mine drainage (AMD) systems. High temperatures associated with wildfires could lead to a sudden schwertmannite transformation, changing the mobility of metal(oid)s. The objective of the present study was to examine the thermal transformation from schwertmannite to hematite, and the subsequent effect on the chromium partitioning. The immobilization of arsenate after thermal transformation and its implications on chromium mobility was also evaluated. Natural schwertmannite, with increasing contents of chromium, was thermally treated between 200 to 800 °C. Transformation products were characterized by solid-phase techniques and selective chemical extractions. Results indicated a transformation to hematite at temperatures above 400 °C. The presence of chromium barely affected the temperature at which the transformation occurred, although partitioning of chromium in the mineral changed with temperature. As the temperature increased from 25 °C to 400 °C, chromium was less mobile and less outcompeted by arsenic adsorption, suggesting a larger contribution of inner-sphere complexes with increasing temperature. At temperatures above 600 °C, non-mobile forms strongly associated with neo-formed hematite were found. Finally, neo-formation of hematite led to a decrease in arsenic adsorption, implying a potentially enhanced arsenic mobility in AMD systems upon wildfires.

**Keywords:** acid mine drainage; schwertmannite; hematite; thermal transformation; chromium; arsenic; adsorption



**Citation:** Lázaro, C.; Antelo, J.; Carabante, I.; Otero-Fariña, A.; Verdes, P.V.; Dacunha-Marinho, B.; Fiol, S. Thermal Transformation of Natural Schwertmannite in the Presence of Chromium. *Minerals* **2022**, *12*, 726. <https://doi.org/10.3390/min12060726>

Academic Editors: Sirio Consani, Teresa Valente, Sergio Carrero Romero and Jakub Kierczak

Received: 30 March 2022

Accepted: 2 June 2022

Published: 6 June 2022

**Publisher's Note:** MDPI stays neutral with regard to jurisdictional claims in published maps and institutional affiliations.



**Copyright:** © 2022 by the authors. Licensee MDPI, Basel, Switzerland. This article is an open access article distributed under the terms and conditions of the Creative Commons Attribution (CC BY) license (<https://creativecommons.org/licenses/by/4.0/>).

## 1. Introduction

Schwertmannite is a poorly crystalline metastable Fe(III)-oxyhydroxysulfate mineral  $(\text{Fe}_8\text{O}_8(\text{OH})_{8-2x}(\text{SO}_4)_x)$ , where  $1 < x < 1.75$ ) that is formed by abiotic and biotic pathways [1–4]. Due to the mechanism that naturally originates schwertmannite, this mineral does mainly occur in soils affected by acid mine or rock drainage, in acid sulfate soils or locations where the oxidation of sulfide minerals is likely to occur. The unique surface and structural properties of schwertmannite propitiate its key role in the speciation and mobility of several oxyanions of environmental interest, such as arsenate, chromate, phosphate, and selenate [1,5,6], through interactions of different nature: anionic exchange with structural  $\text{SO}_4$ , surface complexation with iron hydroxyl groups, or co-precipitation during schwertmannite formation. Under certain circumstances, schwertmannite tends to

transform into more stable phases, such as jarosite, goethite, or lepidocrocite [1,7–9]. This transformation can take between a few weeks and several months, depending on the pH, the oxidizing conditions, and the presence of other species in the medium. The presence of Fe(II) or the increase in temperature, as well as the presence of some types of bacteria, are some of the factors that can accelerate the process, reducing the transformation time to several hours. On the other hand, the presence of sorbed or co-precipitated ions may decrease the transformation rate.

Hexavalent chromium, Cr(VI), which exists in solution as an oxyanion, is a highly mobile and toxic trace metal of great concern due to the environmental and human health risks that it poses [10]. In chromium-polluted areas, Cr(VI) can co-precipitate or adsorb to iron oxide minerals, which show great potential as naturally occurring pollution attenuators due to their high surface area, high point of zero charge (PZC), porous structure, and high density of surface sites [11–14]. Specifically, in AMD systems schwertmannite can act as a specially good scavenger for Cr(VI) species [5,15,16]. In these acidic systems an anion exchange mechanism makes this oxyhydroxysulfate mineral very prone to interacting with anionic species of Cr(VI), thus reducing their mobility. On the other hand, the incorporation of Cr(VI) or other anions into the structure of schwertmannite during its formation can affect the long-term stability of the mineral. Regenspurg and Peiffer [15] confirmed that arsenate and chromate ions stabilize the schwertmannite structure, thus hindering its transformation into more stable crystalline phases that might release the oxyanions back into the solution. Fan et al. [17] and Choppala et al. [18] also found that the substitution of structural sulfate by Cr(VI) ions reduces the Fe(II)-induced transformation of schwertmannite to goethite. As mentioned above, temperature is one of the factors affecting the transformation and stability of schwertmannite, which is a very plausible scenario in areas under climatic or seasonal conditions that favor severe wildfires or bushfires [19]. The changes in schwertmannite mineralogy due to thermal transformation during wildfires will affect the fate of co-precipitated trace elements. The obtention of goethite and hematite as the final products after thermal transformation of ferrihydrite and schwertmannite has been previously reported [19–21]. Johnston et al. [19] reported that above 600 °C, the SO<sub>4</sub> of schwertmannite volatilizes, thus promoting the transformation to hematite and that the structural As initially coprecipitated with schwertmannite can be re-adsorbed by the neoformed hematite as exchangeable surface complexed As, thus reducing its re-mobilization. There is also evidence of goethite transformation to maghemite following a path different from oxidation of magnetite due to bushfire on acid sulfate soil in the presence of organic litter [22]. Vithana et al. [20] investigated the role of co-precipitated ions and temperature on the stability of iron oxides commonly found in acid sulfate soils and AMD systems. They observed different behavior depending on the incorporated species within schwertmannite and ferrihydrite. Thus, thermal transformation enhances the mobility of P or Cu incorporated into schwertmannite but, on the other hand, strongly inhibits the mobility and bioavailability of Sb.

What remains clear is that schwertmannite can act either as a sink or a source of different metals and metalloids upon thermal transformation. Therefore, it is still necessary to investigate and understand the consequences that wildfires or bushfires can provoke in the stability of iron minerals and the implication on the fate of contaminants in the environment. To contribute to such knowledge, the objective of the present work is to provide further information on how fire can affect the remobilization of chromate chemically bound to the surface of a natural schwertmannite sample formed under AMD conditions. To that end, different loadings of Cr(VI) were used in Cr-schwertmannite adsorption experiments. Schwertmannite samples with and without Cr were subjected to thermal treatment at different temperatures to simulate the effect of the intensity of wildfires in the mobilization of chromate. The solids were analyzed for possible mineralogical changes through XRD, ATR-FTIR, TGA, and chemical analysis by selective Fe and Cr extractions. In addition, the ability of this AMD-schwertmannite sample to remove arsenate from solution was determined in the presence and absence of Cr. The results indicate that at low

to intermediate temperatures schwertmannite and ferric sulfate minerals predominated, whereas neo-formed hematite dominated at higher temperatures. The partitioning of Cr changed with temperature, becoming progressively stabilized. Moreover, the efficiency of schwertmannite to remove arsenic from solution decreased as the temperature increased.

## 2. Materials and Methods

### 2.1. Field Site and Sampling

AMD samples were collected from an abandoned copper mine in Touro (NW Spain, 42° 52' 34" N 8° 20' 40" W), which was operational between 1974 and 1988. The main minerals found at the mine include pyrite, chalcopyrite, and pyrrhotite. The mining activities and the exposure of the sulfide minerals to the atmosphere led to AMD episodes, affecting the rivers and streams surrounding the mine [23,24]. In the last 15–20 years, several remediation efforts and continuous environmental monitoring have been conducted at the most critical sites in the mining area [25,26].

AMD water and iron-rich AMD bed sediment samples were collected at the Portapego stream, which crosses through the mine of Touro, in March 2015. The water sample, POR<sub>w</sub>, was filtered through 0.45 µm Millipore filters and subsamples were acidified with 1% HCl or HNO<sub>3</sub> for subsequent analysis of the concentrations of Fe(II) and total metals, respectively [27]. Analysis of pH, electrical conductivity, redox potential, and temperature was conducted in situ with a multiparameter probe (Hach HQ40d). Then, samples were transported to the laboratory and stored in the dark, at 4 °C, until analysis. The total concentration of metals was determined by inductively coupled plasma-optical emission spectrometry (ICP-OES, Perkin–Elmer Optima 3300DV). The concentration of Fe(II) was determined by the 1,10-phenantroline method, whereas the sulfate concentration was determined by a turbidimetric standard method [28].

The bed sediment sample, POR<sub>s</sub>, was collected from the surface layer (0–10 cm) and transported to the laboratory in polyethylene bottles at 4 °C. The sample was dried at room temperature, sieved to 63 µm, and ground to obtain a homogenous powder for solid characterization and subsequent experiments. The chemical composition of the solid sample was determined following microwave-assisted acid digestion with aqua regia. The solution obtained was diluted with ultrapure water and the concentration of major and trace elements (Fe, Al, Cu, Ni, Zn, and S) was determined by ICP-OES. Solid samples were also characterized by X-ray diffraction (XRD), thermogravimetric analysis (TGA), and attenuated total reflectance Fourier transform infrared (ATR-FTIR) spectroscopy (described below in Section 2.4).

### 2.2. Preparation of Cr(VI)-AMD Samples

The AMD bed sediment, POR<sub>s</sub>, was used to prepare subsamples with different Cr(VI) contents following a similar procedure to that described by Antelo et al. [5] for the adsorption of chromate on schwertmannite. Briefly, adsorption experiments were conducted at pH 3, using 10 g/L suspensions in 0.1 M KNO<sub>3</sub> as inert electrolyte. The total chromate concentration added to the suspensions was 0.17 mM (POR\_Cr1), 1.7 mM (POR\_Cr2), and 17 mM (POR\_Cr3), corresponding to Cr/Fe molar ratios of 0.002, 0.02, and 0.2, respectively. Once chromate was added to the AMD suspensions, the pH was adjusted to 3 by the addition of 0.1 M HNO<sub>3</sub> or KOH solutions and the samples were equilibrated for 72 h. During the equilibration period, the samples were continuously shaken with a magnetic stirrer, and the pH was periodically measured and readjusted when necessary. Samples were then centrifuged (6000 rpm for 15 min) and filtered (0.45 µm Millipore filters). The concentration of chromate in the solution was determined by the diphenylcarbazide method [29], and in the solid sample was determined as the difference between the initial concentration added and the final concentration in the solution. The solid samples obtained were washed with ultrapure water and centrifuged to remove the ionic species present in the solution. After three washing cycles, the suspensions were freeze-dried in order to obtain powder solid samples for further experiments.

### 2.3. Thermal Transformation Products

The thermal transformation of the solid samples (with and without Cr(VI)) was conducted in a muffle furnace (SEL-HORN “R-8 L”) under an air atmosphere. The conditions were similar to those proposed by Johnston et al. [19]; 5 g of dried samples were heated in ceramic crucibles for 4 h at 200, 400, 600, and 800 °C. These temperatures were selected considering the range of soil temperatures than can occur during wildfire or bushfire episodes [30,31]. After the thermal treatment, the solid samples were cooled at room temperature and ground in order to obtain a fine powder. These samples were characterized following a similar methodology as for the AMD sediment sample.

### 2.4. Solid Characterization

Powder X-ray diffraction (XRD) was measured with a Phillips PW1710 diffractometer between 15° and 65° 2 $\theta$ , with a step size of 0.02° and counting time of 3 s per step. The crystal phase matching (with 2011-PAN ICSD crystal database) and the mathematical fitting of experimental diffractograms was conducted using the software PANalytical-HighScore Plus. The peak function was refined using the Pseudo Voigt model and the background contribution was refined using an order 4 polynomial fitting.

Thermogravimetric analysis (TGA) was conducted with a Perkin-Elmer STA 6000. Samples were heated under nitrogen atmosphere (20 mL/min) from 30 °C to 1000 °C, with a temperature ramp of 5 °C/min. The resulting data were manipulated using Pyris thermal analysis software v11.1.

ATR-FTIR measurements were taken with a JASCO FTIR-4200 spectrometer using a ZnSe ATR crystal plate (Pike MIRacle Single Reflection ATR). The spectra of the solid samples were collected with a scan resolution of 2 cm<sup>-1</sup>, with a minimum of 50 scans per sample.

### 2.5. Selective Extractions

Separate selective extractions were conducted to identify different operational defined phases present in the thermally transformed products, following a similar approach as Johnston et al. [19] and Vithana et al. [20]. Table 1 summarizes the chemical extractants and reaction times for each selective extraction, along with the fractions targeted by each extractant and the reference for each method. There is no standardized solid:extractant ratio common to the different selective extractions, although there are two key factors to consider: using enough solid sample to achieve reproducible results and selecting an adequate extractant volume to ensure complete extraction of the target element [32]. In the present study a solid:extractant ratio of 1:100 was used. For each selective extraction procedure, after the corresponding equilibration time, samples were centrifuged at 6000 rpm and the supernatant was filtered through 0.45  $\mu$ m Millipore filters. The concentration of Fe and Cr in the filtrates was measured by ICP-OES. The percentage of Fe and Cr dissolved from the solid in each selective extraction was normalized to the total concentration extracted by aqua regia.

**Table 1.** Main features of the selective extraction procedures for Fe and Cr.

Extractant	Reaction Time	Phase Justification	Reference
1 M MgCl <sub>2</sub>	1 h	Exchangeable or ionically bound to the mineral surface (Cr <sub>exc</sub> )	[32]
1 M NaH <sub>2</sub> PO <sub>4</sub>	16 h	Strongly adsorbed on the mineral surface (Cr <sub>ads</sub> )	[33]
0.2 M citrate/0.4 M ascorbate	24 h	Associated with poorly crystalline mineral phases (Cr <sub>cit</sub> and Fe <sub>cit</sub> )	[34]
1 M HCl	4 h	Coprecipitated with carbonates, Mn oxides, and poorly crystalline Fe oxyhydroxides (Cr <sub>HCl</sub> and Fe <sub>HCl</sub> )	[32]
Aqua regia	16 h	Total concentration of iron and chromium present in solid phases (Cr <sub>tot</sub> and Fe <sub>tot</sub> )	[28]

## 2.6. Arsenic Adsorption Experiments

Batch adsorption experiments at constant pH were conducted with the sediment sample (POR<sub>S</sub>), all the Cr(VI)-coprecipitated AMD samples (POR\_Cr1, POR\_Cr2, and POR\_Cr3), and the corresponding thermal transformation products obtained between 200 and 800 °C. Suspensions of 1 g/L were prepared in 0.1 M KNO<sub>3</sub>, as inert electrolyte, in 50 mL polyethylene flasks, to which aliquots of a 40 mM KH<sub>2</sub>AsO<sub>4</sub> stock solution were added to have total arsenate concentrations of 0.17 and 1.7 mM. Once arsenate aliquots were added to the suspensions, the pH was adjusted to 3 by the addition of 0.01 or 0.1 M HNO<sub>3</sub> and samples were shaken on an end-over-end shaker for 72 h to ensure equilibrium [5]. During the equilibration period, the pH was periodically measured and readjusted if necessary. The samples were then filtered (0.45 µm Millipore filters) and the concentration of arsenate in the filtrate was determined by a colorimetric method [35]. The concentration of adsorbed arsenate was calculated as the difference between the total concentration and the concentration measured in the solution. Finally, the concentration of chromate released to the solution upon arsenate adsorption was also measured by ICP-OES.

All chemicals were of Merck pro analysis grade (p.a.) and the water used in the experiments was ultrapure and CO<sub>2</sub> free. Polyethylene flasks were used in the experiments in order to avoid contamination by silicates.

## 3. Results and Discussion

### 3.1. Characterization of AMD

#### 3.1.1. AMD Aqueous Chemistry

The in situ measurements and the chemical composition of the water sample, POR<sub>w</sub>, indicate that the study site is affected by AMD (Table 2), as is reflected by the low pH, 3.34, and the high concentrations of Fe(II) and SO<sub>4</sub>, 309 and 2485 mg/L, respectively. The acidic pH and high SO<sub>4</sub> concentration were caused by the oxidation process of pyrite or any other mineral sulfide present in the system. The concentration of the trace elements analyzed exceeded the average values found in unaffected surface waters, generally lower than 1 µg/L, and are comparable to the concentration found for other AMD sites [36].

**Table 2.** Physico-chemical characteristics of the AMD water samples.

pH	EC	Eh	T	Fe <sub>tot</sub>	Fe(II)	Al	Cu	Zn	Ni	Mn	SO <sub>4</sub>
	µS/cm	mV	°C				mg/L				
3.34	1856	297	16.7	365.4	309	12.9	0.09	0.16	0.20	13.5	2485

#### 3.1.2. Chemical and Mineralogical Composition of AMD Precipitate

The AMD precipitate, POR<sub>S</sub>, was characterized by XRD and ATR-FTIR. The X-ray diffractogram (Figure 1a) showed five broad peaks assigned to the presence of schwertmannite, being the most characteristic and intense the peak located at ~35° 2θ. The presence of schwertmannite confirmed the affection of the sampling site by AMD, since this mineral is dominant in systems with a pH in the range of 3–4 and with high concentrations of SO<sub>4</sub> [3]. The presence of a peak at ~27° 2θ may be associated with the presence of quartz, whereas the low-intensity peaks observed at ~17.9° and ~45.6° 2θ may be associated with the formation of jarosite. The ATR-FTIR spectra centered in the region of 1300–700 cm<sup>-1</sup> (Figure 2) showed bands associated with sulphate vibrations (S-O stretching bands) [37]. The bands at ~1100 and ~1042 cm<sup>-1</sup> might be associated with asymmetric stretching (ν<sub>3</sub>), and the band at ~971 cm<sup>-1</sup> with symmetric stretching (ν<sub>1</sub>). Splitting into separate ν<sub>3</sub> bands is common for iron oxyhydroxysulfate minerals formed at an acidic pH, which is indicative of the presence of inner-sphere sulphate complexes [23,38]. When the presence of outer-sphere complexes dominates, no peak splitting is observed. Besides the bands associated with sulphate vibrations typical of schwertmannite, two bands associated with δ<sub>OH</sub> and γ<sub>OH</sub> present in goethite [37] appeared at 890 and 795 cm<sup>-1</sup>. It should be kept in

mind that due to the metastable character of this mineral phase, a partial transformation from schwertmannite to goethite could be occurring at field conditions in medium- to long-term time scales [1].

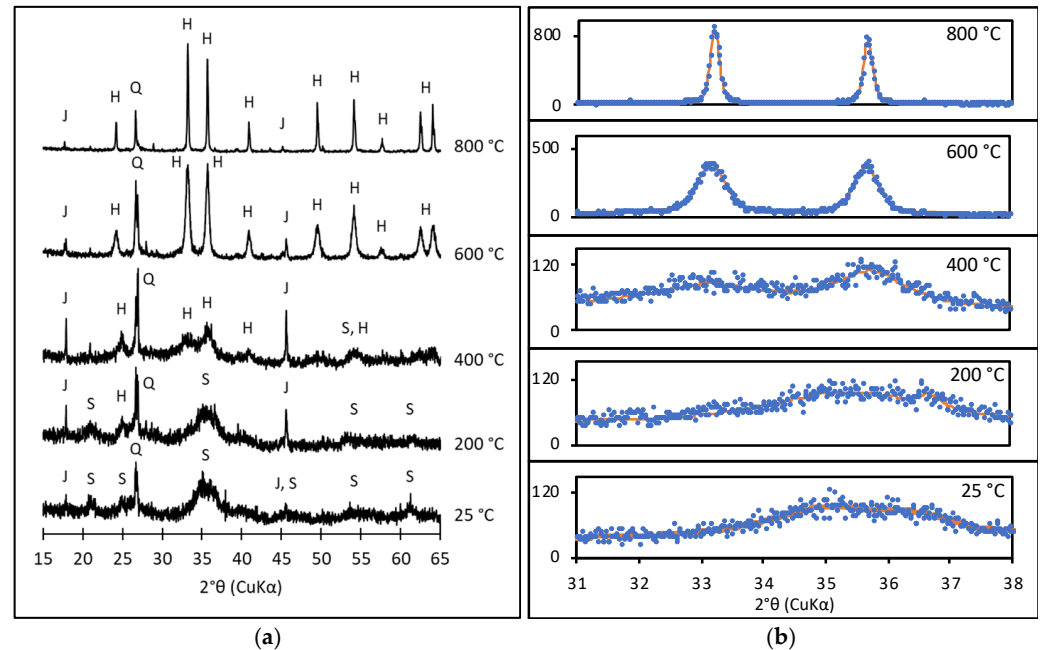


**Figure 1.** (a) X-ray diffractograms of sample POR<sub>5</sub> and the thermal transformation products obtained at 200, 400, 600, and 800 °C. H = hematite; J = jarosite; Q = quartz; S = schwertmannite. (b) Detail of the XRD region between 31° and 38° 2 $\theta$  showing the evolution of the main peaks associated with the schwertmannite–hematite transformation.

The chemical analysis of POR<sub>5</sub> indicates that the main components were Fe and SO<sub>4</sub>, with concentrations 8.59 and 1.79 mmol/g, respectively. The high concentration of Fe compared with Al (0.40 mmol/g), along with the acidic pH of the system (2.59), favors the precipitation of Fe phases rather than Al phases [39]. The sulfate content was slightly above the concentration range proposed by Bigham et al. [2], but within the values proposed by Caraballo et al. [40]. The Fe:S ratio was 4.80, which agrees with the values obtained for natural schwertmannite originating in AMD systems (3.10–10.62) [40]. This composition allows a chemical formula to be proposed for the POR<sub>5</sub> sample: Fe<sub>8</sub>O<sub>8</sub>(OH)<sub>4.67</sub>(SO<sub>4</sub>)<sub>1.67</sub>. Despite the sampling site being in an abandoned copper mine, no significant concentrations of copper were detected ( $6.92 \times 10^{-4}$  mmol/g), similar to other natural schwertmannite samples collected in different locations [41]. Other trace elements were below detection limits.

### 3.2. Characterization of Cr(VI)-AMD Samples

The ability of schwertmannite to incorporate Cr(VI) ions into its structure is limited by the content of sulfate present, since the dominant adsorption mechanism is, in this case, the anion exchange between structural SO<sub>4</sub> and CrO<sub>4</sub> [5,16]. Despite the high concentration of sulfate in the POR<sub>5</sub> sample, not all the Cr(VI) added in the sorption experiments was incorporated into the schwertmannite, independently of the Cr/Fe molar ratio selected. This also happens with the incorporation of other elements, such as Cu and As, to synthetic schwertmannite through coprecipitation processes [15,42]. The final concentrations of incorporated Cr were 5.64, 47.88, and 194.91  $\mu$ mol/g for POR\_Cr1, POR\_Cr2, and POR\_Cr3, respectively (Table 3). This Cr concentration was highly correlated to the SO<sub>4</sub> concentration in the samples. SO<sub>4</sub> to Cr ratio was below 1 (theoretical anion exchange ratio in schwertmannite [5]) due to desorption of the weakly bound Cr during the washing of the solid. XRD diffractograms of these samples were similar to those of the precursor sample (POR<sub>5</sub>) (Figure S1 in Supplementary Materials), showing the characteristic peaks

of schwertmannite without significant changes in their position or intensity. The incorporation of Cr(VI), as chromate ions, did not modify the crystalline structure of the original schwertmannite sample.

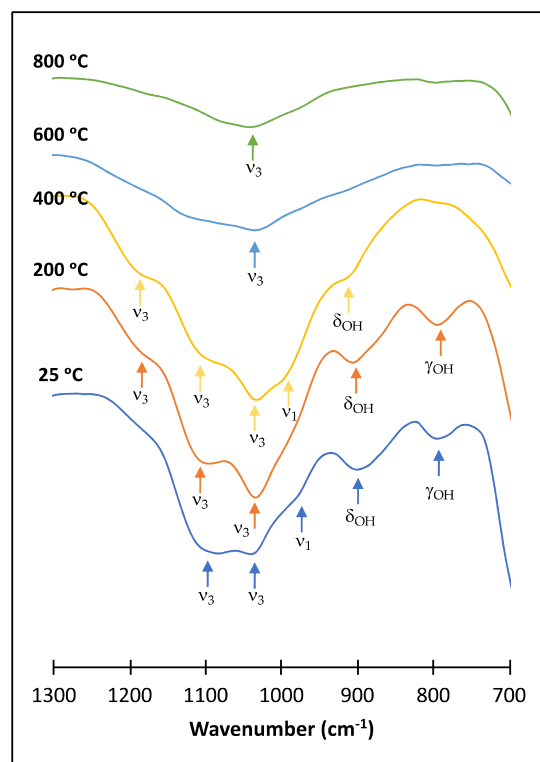


**Figure 2.** ATR-FTIR spectra (region 1300 to 700  $\text{cm}^{-1}$ ) of the AMD sample,  $\text{POR}_s$ , and the corresponding thermal transformation products.  $\nu_3$  and  $\nu_1$  correspond to the asymmetrical and symmetrical stretching of S-O, respectively;  $\delta_{\text{OH}}$  and  $\gamma_{\text{OH}}$  correspond to O-H deformations.

**Table 3.** Chemical composition of Cr(VI)-AMD samples.

Sample	Fe mmol/g	$\text{SO}_4$ mmol/g	Cr $\mu\text{mol/g}$
$\text{POR}_s$	8.59	1.79	-
POR-Cr1	6.98	1.50	5.64
POR-Cr2	6.71	1.28	47.88
POR-Cr3	7.27	0.71	194.91

### 3.3. Thermal Transformation Products

Thermal transformation of poorly crystalline iron oxides, such as schwertmannite, leads to the formation of more stable crystalline phases, such as goethite and hematite. Figure 1a shows the evolution of the XRD patterns with the temperature for sample  $\text{POR}_s$ . The characteristic peaks of schwertmannite appeared in the samples at 25 °C, as previously indicated, and at 200 °C, although in the latter the presence of incipient peaks at  $\sim 17.9^\circ$  and  $\sim 45.6^\circ$   $2\theta$ , which are typical of jarosite, were found as a consequence of a possible rearrangement of the crystal lattice. At 400 °C, the characteristic broad peak of schwertmannite, found at around  $\sim 35^\circ$   $2\theta$ , split into two new peaks that can be assigned to hematite formation. Additionally, the peaks characteristic of jarosite increased their intensity. These results agree with those described by Vithana et al. [20] for synthetic schwertmannite, who reported the formation of poorly crystallized hematite above 300–400 °C. At temperatures above 400 °C changes in mineralogy were significant, additional peaks were observed,

and all the peaks became better defined, narrower, and more intense, indicating a higher crystallinity degree of the mineral phases (Figure 1b). Thus, between 600 and 800 °C, peaks associated with neo-formed hematite became increasingly clearer, which also agrees with results found in previous studies [20]. Thermal transformation occurs via an initial dehydration and dehydroxylation stage at low to intermediate temperatures, leading to the formation of  $\text{Fe}_2(\text{SO}_4)_3$ , followed by the release of structural sulphate as  $\text{SO}_2$  or  $\text{SO}_3$  at temperatures above 500–600 °C, and the decomposition of  $\text{Fe}_2(\text{SO}_4)_3$  and the formation of hematite ( $\text{Fe}_2\text{O}_3$ ) [2,3].

The evolution with temperature of the XRD patterns for the Cr-samples is presented in Figure S2 (Supplementary Material). The presence of Cr barely affected the mineralogy of the intermediate and final products formed during the thermal transformation process, similar to other elements [20]. Regardless of the Cr loading in the samples, the final product obtained in all cases was hematite. At 200 °C, the diffractograms of the samples, with and without Cr, showed mainly the bands of schwertmannite. As the temperature rose to 400 °C, the characteristic peaks of hematite also began to develop in the Cr-samples, although these were better defined in samples with lower Cr loadings (POR\_Cr1 and POR\_Cr2). The hematite peaks were observed in all samples obtained at 600 and 800 °C. At these higher temperatures, no shift in the reflection peaks of hematite was observed (Figure S3, in Supplementary Material), thus suggesting that Cr was not incorporated into the hematite crystalline structure. Although schwertmannite predominated below 400 °C and hematite above this temperature, peaks associated with a third iron mineral phase, i.e., jarosite, were also observed in the diffractograms of all samples, with less-developed peaks for the POR\_Cr3 sample. To further investigate the influence of Cr(VI) on the thermal transformation from schwertmannite to hematite, a more detailed analysis of the position and full width (at half maximum, FWHM) of representative peaks of both hematite and schwertmannite in three different regions of the diffractogram ( $2\theta$  values of 24–25°, 35–37° (Figure 1b), 53–54.5°) was conducted. The results of the mathematical analysis of the peak positions and FWHM from XRD are shown in Supplementary Materials (Figure S3). At intermediate temperatures of 200–400 °C, a higher distortion of schwertmannite nanocrystals was observed with increasing Cr loadings, whereas no significant change was observed at higher temperatures of 600–800 °C. The slight change in thermal stability of schwertmannite may have been caused by the previous release of structural sulphate due to the sulphate–chromate exchange reactions.

Figure 2 and Figure S4 (in Supplementary Materials) show the ATR-FTIR spectra obtained for the AMD iron oxide,  $\text{POR}_S$ , and the thermal transformation products obtained between 200 and 800 °C. During the thermal transformation some changes affected the ATR-FTIR spectra in two different regions. The first change corresponded to the band centered at  $3150\text{ cm}^{-1}$ , associated with water bending and stretching O-H vibrations from iron oxyhydroxysulfates (Figure S4 in Supplementary Material). The increase in temperature produced a reduction in the intensity of this band that corresponded to the water loss in the sample due to dehydration and dehydroxylation reactions. Dehydration of sorbed or surface water on schwertmannite occurs at a lower temperature range, around 100 °C, as demonstrated by Boily et al. [37], whereas dehydration and dehydroxylation of structural  $\text{H}_2\text{O}$  and OH groups take place at up to 300 °C [3]. The absence of this band at the highest temperature range agrees with the X-ray diffractograms obtained above 600 °C, where hematite ( $\text{Fe}_2\text{O}_3$ ), a mineral phase exempt of water in its structure, dominated. The second change was observed at the region between  $1300$  and  $700\text{ cm}^{-1}$ . As mentioned above, the  $\text{POR}_S$  sample presented bands characteristic of goethite at  $890$  and  $795\text{ cm}^{-1}$ , which disappeared above 200 °C. The most relevant change occurred in the bands associated with sulfate vibrations (S-O stretching bands at  $\sim 1100$ ,  $1042$ , and  $971\text{ cm}^{-1}$ ), which are typical of schwertmannite. As the temperature increased the intensity of these bands decreased, especially at temperatures between 600 and 800 °C. As stated above, at intermediate temperatures the removal of structural  $\text{H}_2\text{O}$  and OH may have led to a structural rearrangement of schwertmannite and to the formation of  $\text{Fe}_2(\text{SO}_4)_3$ .

The vibrational S-O bands for the ferric sulfate were found within the same wavelength range as schwertmannite, with the most relevant signals found at 1193, 1106, 1053, and 1033  $\text{cm}^{-1}$  [43]. When the temperature increased structural sulfate was released as  $\text{SO}_2$  or  $\text{SO}_3$ , and schwertmannite (or the intermediate ferric sulfate phase) was partially or completely transformed to hematite.

Weight-loss curves and the corresponding derivative of the weight-loss as a function of temperature are shown in Figure 3. In Table S1 (Supplementary Materials), data of the weight-loss percentage for the different peaks are collected. The thermogravimetric curves had three regions that corresponded to surface-sorbed  $\text{H}_2\text{O}$ , structural  $\text{H}_2\text{O}$  and OH, and structural  $\text{SO}_4$  loss from the mineral. Between 30 and 300 °C two weight-loss peaks were observed for the four samples (with and without Cr) and amounted up to 23% of the initial weight due to the loss of adsorbed water and structural OH/ $\text{H}_2\text{O}$  groups. The corresponding differential curves showed a peak associated with each fraction, i.e., at 105 °C it was associated with water loosely adsorbed or non-structural water trapped in the interstitial spaces of aggregated particles, and at 260 °C, corresponding to structural OH/ $\text{H}_2\text{O}$  associated with changes in the schwertmannite crystalline phase that may eventually lead to the formation of a ferric sulfate phase. Each fraction represents a weight loss of 2.8–4.3% and 17–19%, respectively. These weight-loss peaks were also found in previous studies when conducting thermogravimetric analysis of natural and synthetic schwertmannite samples [3,44]. A third weight-loss peak was found between 400 and 700 °C, centered at ~615 °C, and can be assigned to the release of structural sulfate in the form of  $\text{SO}_2$  or  $\text{SO}_3$  [2,3]. In the case of the POR\_Cr3 sample, this peak shifted towards a slightly higher temperature, ~622 °C, which could be attributed to small differences in the crystallinity degree of the samples [44]. Although the peaks associated with sorbed or structural water showed no difference between samples with and without Cr, this third peak showed a decrease in the weight loss with the increase in the Cr content in the sample. Thus, for the sample without Cr, POR<sub>5</sub>, weight loss was ~9.8% and for the sample with the highest Cr loading, POR\_Cr3, it was ~5.3%. This difference can be attributed to the substitution of structural  $\text{SO}_4$  by  $\text{CrO}_4$  during the Cr(VI) adsorption. As previously stated, the incorporation of  $\text{CrO}_4$  to schwertmannite is mainly caused by an anion exchange mechanism [5]; therefore, as the concentration of Cr in the sample increased the content of  $\text{SO}_4$  decreased (Table 3). The behavior observed in the TGA curves agrees with the ATR-FTIR spectra, which showed a decrease in the intensity of the bands associated with structural  $\text{SO}_4$  as the temperature increased from 400 to 800 °C. On the other hand, the weight loss due to the dehydration and dihydroxylation, below 400 °C, was reflected by the decrease and complete disappearance of the band associated with the OH stretch ( $\nu_{\text{OH}}$ ) present in the FTIR spectra ( $3150 \text{ cm}^{-1}$ ).

### 3.4. Partitioning of Iron and Chromium in Thermal Transformation Products

Changes in temperature of the Fe and Cr extractability in the transformation products are shown in Figure 4. At low to intermediate temperatures, below 600 °C, a major fraction of the Fe was extracted with 1 M HCl, ~80% of the total Fe, irrespective of the Cr concentration in the sample (Figure 4a). This agrees with the XRD data for the natural sample and the transformation products obtained at 200 and 400 °C, in which schwertmannite was the main phase identified (Figure 1). A fraction of the poorly crystalline Fe was also extracted by the citrate/ascorbate solution, although the concentration extracted varied with the temperature and with the Cr concentration. Thus, the contribution of this extract increased from ~10–30% to ~60–80% of total Fe as the temperature increased from 25 to 400 °C. The contribution of citrate/ascorbate extractable Fe in samples at 400 °C is noteworthy, since the amounts were similar to those extracted with 1 M HCl. Both solutions were intended to extract elements associated with poorly crystalline mineral phases, although in the case of Fe the solution of 1 M HCl seemed to be more efficient [19]. The presence of Cr produced a slight decrease in the citrate/ascorbate extractable Fe, e.g., from ~30% in sample without Cr to ~10% in the sample with the highest Cr content at 25 °C. This could be attributed to

a stabilizing effect on the schwertmannite due to the presence of  $\text{CrO}_4$  in the crystalline structure, which was introduced through  $\text{SO}_4\text{-CrO}_4$  exchange. At higher temperatures, transformation from schwertmannite to hematite coincided with a large decrease in the concentration of Fe extractable by either citrate/ascorbate or 1 M HCl. In the samples thermally transformed at 600 and 800 °C, most of the Fe could only be extracted with aqua regia, whereas the other extractants were only able to produce 5% total Fe, which reveals the high crystallinity degree of the neo-formed hematite. This agrees with the results found for synthetic schwertmannite by Johnston et al. [19] and Vithana et al. [20] when studying its thermal transformation. They also reported the transition from Fe associated with schwertmannite particles towards neo-formed hematite particles at temperatures above 400–500 °C.

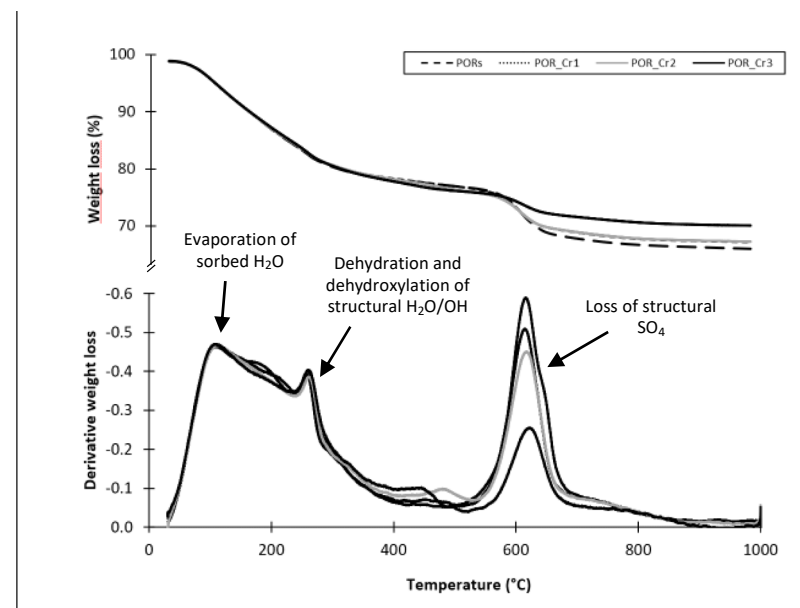


**Figure 3.** TGA results for the AMD sample  $\text{POR}_s$  and the corresponding thermal transformation products. Upper curves represent the percent weight loss measured during heating. Lower curves correspond to the derivative of the weight-loss curves as a function of temperature.

Partitioning of Cr with temperature showed marked differences for samples  $\text{POR}_{\text{Cr}1}$ ,  $\text{POR}_{\text{Cr}2}$ , and  $\text{POR}_{\text{Cr}3}$  (Figure 4b). Cr was mainly found in three different forms, bound or sorbed to the mineral surface, associated with the poorly crystalline fraction, and associated with the crystalline fraction of the mineral. These forms accounted for ~80% or more of the total extractable Cr and represented effectively immobilized Cr. Similar to Fe, the main fraction of Cr below 400 °C was associated with poorly crystalline phases and was extracted with 1 M HCl. The amounts extracted from this phase decreased when increasing the temperature from 25 to 400 °C. On the other hand, the fraction of Cr extractable with the reducing solution of citrate/ascorbate increased as the temperature increased from 25 to 400 °C, agreeing with the behavior observed for Fe. At low to intermediate temperatures, a minor fraction of Cr was extracted with 1 M  $\text{MgCl}_2$  and 1 M  $\text{NaH}_2\text{PO}_4$  solutions, corresponding to exchangeable Cr or strongly sorbed Cr, respectively. Thus, at 25 °C, for sample  $\text{POR}_{\text{Cr}1}$ , ~16% of the extractable Cr was found in strongly sorbed forms, i.e., extracted by  $\text{NaH}_2\text{PO}_4$ . On the contrary, for the sample with the highest content of Cr,  $\text{POR}_{\text{Cr}3}$ , a similar percentage of extractable Cr was present in exchangeable forms and was extracted by  $\text{MgCl}_2$ . For an intermediate Cr loading,  $\text{POR}_{\text{Cr}2}$ , a combination of both extractants was necessary to get the same percentage of Cr. The increase in temperature resulted in a progressive reduction of the Cr extracted in the more mobile forms, from ~20% to less than ~5% at 400 °C. Above 600 °C, Cr was repartitioned and present mainly as non-mobile or stabilized forms, since the concentration of exchangeable or surface-sorbed Cr

became negligible. In addition, the contribution of Cr associated with the poorly crystalline iron phases was also non-significant at 600 to 800 °C. Therefore, at high temperatures Cr must be strongly stabilized within the structure of the neo-formed hematite. In general, Cr behaves differently compared to other elements such as As or Cu [19,20]. In the case of As, the extractable fraction increases with temperature, reaching its maximum at 800 °C. This means that an increase in temperature increases As availability. On the contrary, Cr showed a similar behavior to that found for Sb on synthetic schwertmannite, where an increase in temperature led to the disappearance of the extractable fraction [20].

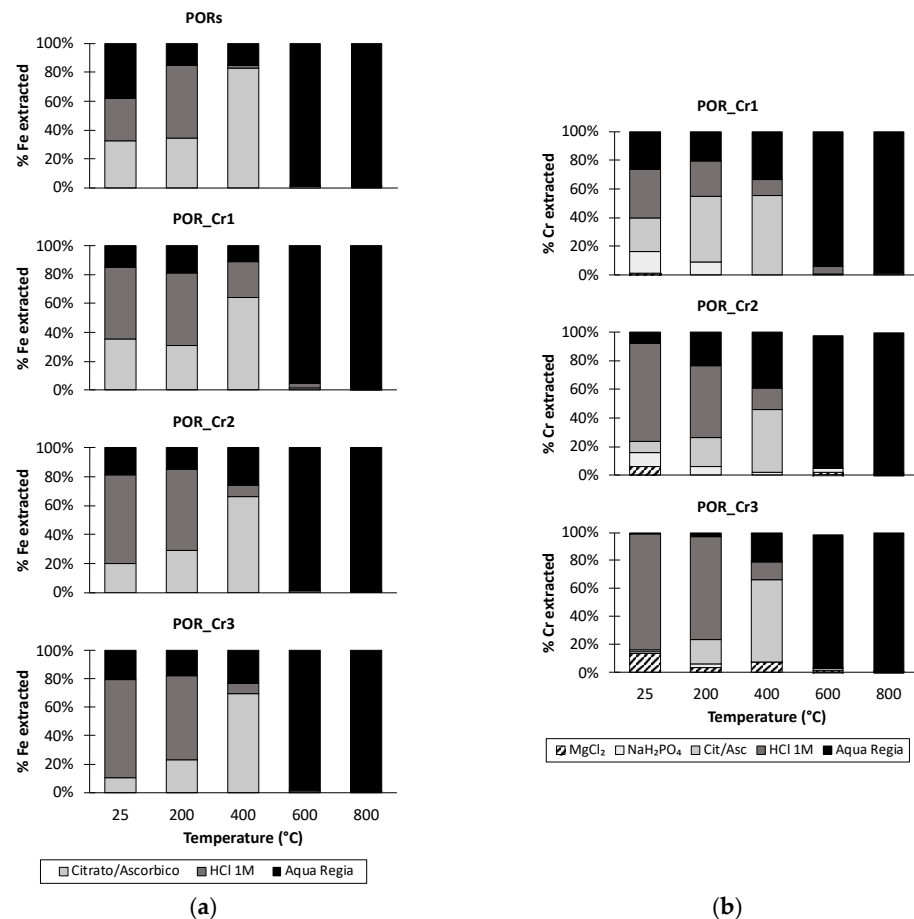


**Figure 4.** Partitioning of (a) Fe and (b) Cr in AMD sample POR<sub>5</sub> and the thermal transformation products.

### 3.5. Arsenate Adsorption Experiments

Adsorption experiments were conducted to evaluate the As adsorption capacity of the natural schwertmannite sample and its thermal transformation products, with and without Cr (Figure 5). These experiments were conducted at pH 3, which is a common pH in acid sulfate soils and AMD-affected systems, where oxyanion adsorption is favored [9,45]. At low As loading (0.17 mM), samples with no thermal treatment, regardless of the presence or absence of Cr, showed a retention capacity of 20–25 mmol AsO<sub>4</sub>/mol Fe (~100%) (Figure 5a). When the As loading was increased tenfold (1.7 mM), the retention capacity increased up to 100–150 mmol AsO<sub>4</sub>/mol Fe (Figure 5b). However, those values are well below the adsorption capacity of synthetic schwertmannite samples in similar conditions, which can reach an adsorption capacity of 190 mmol AsO<sub>4</sub>/mol Fe [5]. Generally, natural samples, such as POR<sub>5</sub>, showed lower reactivity than synthetic analogues, which may have been caused by the existence of other mineral phases with a higher crystallinity or the presence of co-precipitated ions that reduce the surface site availability or change other surface properties [23,45,46].

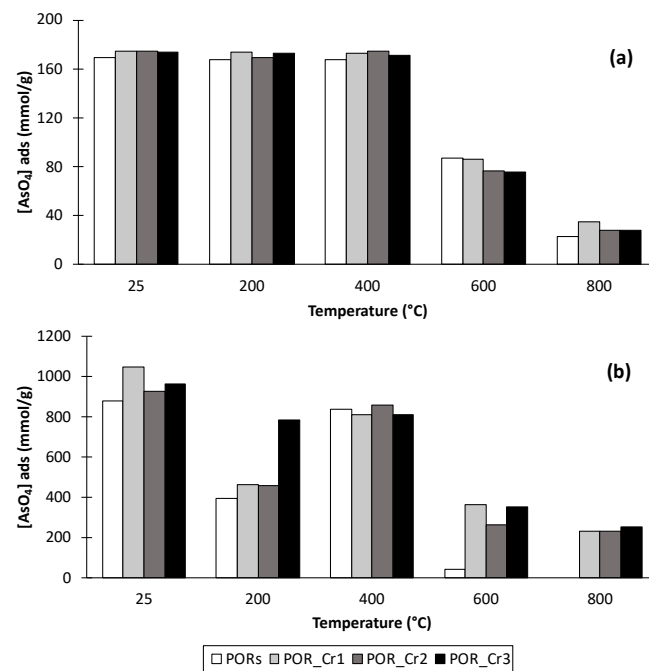


**Figure 5.** Arsenate adsorption in the AMD sample PORs and the thermal transformation products at pH 3 and at different arsenate loadings: (a) 0.17 and (b) 1.7 mM.

A decrease in the As adsorption capacity was observed as the temperature increased. This effect was much clearer at high As loadings (Figure 5b). As previously stated, thermal treatment leads to a phase transformation towards more stable crystalline phases, which is accompanied by a reduction in the oxyanion adsorption capacity. In samples obtained at low–intermediate temperatures, below 400 °C, schwertmannite predominated, whereas hematite would be the predominant mineral phase in samples thermally treated between 600 and 800 °C (Figure 1). The ion adsorption capacity of iron mineral surfaces is related to the degree of crystallinity of the minerals, which is related to the specific surface area or the surface site density. Nano-sized mineral phases, such as schwertmannite, usually show higher surface areas (100–350 m<sup>2</sup>/g [2]). This parameter decreases to values between ~10 and ~70 m<sup>2</sup>/g in iron oxides such as hematite or goethite [47,48]. This might be the main reason why samples obtained at 400 °C or below presented higher values of adsorbed As, 20–25 mmol AsO<sub>4</sub>/mol Fe (low As loading) and 110–150 mmol AsO<sub>4</sub>/mol Fe (high As loading). Above 400 °C, As adsorption decreased to values between 3–8 and 20–35 mmol AsO<sub>4</sub>/mol Fe for the low and high As loadings, respectively. Finally, the increase in reactivity between 200 and 400 °C at the higher As loading, 1.7 mM AsO<sub>4</sub>, is remarkable. Although a decrease would be expected, this fact could be associated with the change observed in the Fe partitioning (Figure 4a). At 400 °C the fraction extracted by the citrate/ascorbate solution, associated with poorly crystalline mineral phases, was significant, 60–80%, whereas at 200 °C this fraction only accounted for 20–30% of total Fe. This significant increase between 200 and 400 °C could explain this behavior in As adsorption.

The presence of Cr in thermally transformed samples barely affected the As retention capacity at low As loading (Figure 5a). However, at high As loading (Figure 5b), the adsorption capacity of the samples without Cr thermally treated at 600 and 800 °C was negligible (<2%). On the other hand, in samples containing Cr thermally treated at these temperatures, the As adsorption reached values between ~13 and 20% and was not affected by changes in the Cr content. As stated above, the thermal transformation products obtained at 200 and 400 °C presented anomalous behavior, since adsorption levels at 200 °C were lower than those found at 400 °C, when the opposite was expected. This effect was ascribed to changes in the Fe partitioning. The only exception was sample POR\_Cr3, showing similar adsorption levels at both temperatures, which cannot be easily explained.

During As adsorption, some chromate was released into the solution (Figure 6). In samples with no thermal treatment, more chromate was released in the presence of higher As concentration, 1.70 mM, and this release was dependent on the initial chromium content. Thus, at low As loading the Cr released to the solution corresponded to 5–35% of the initially sorbed Cr, whereas at high As loading it corresponded to 25–60%. This result supports the existence of an As–Cr competition for the surface sites present in the AMD precipitates. Previous literature results for oxyanion binding to iron oxide surfaces indicate that these surfaces generally show a higher affinity for arsenate than for chromate ions [5,15]. In samples subjected to thermal treatment, the maximum chromate concentrations found in solution upon arsenate adsorption varied between ~6% and ~12% at low and high As loadings, respectively, indicating a lower contribution of As–Cr competition to bind to the mineral surface sites. This behavior can be explained considering the previous results of Cr repartitioning with temperature. At low temperatures, Cr is mostly present as mobile species, whereas at intermediate to high temperatures Cr species become more stabilized and difficult to extract (Figure 4). This behavior was also reflected in the As-adsorption experiments. At 25 °C, the more labile Cr species were easily exchangeable by As. At higher temperatures, this Cr–As exchange became more difficult since the Cr was more unlikely to desorb. Although Cr partitioning changed even before the transformation from schwertmannite to hematite occurred (above 400 °C), there was no directly measured evidence of the forms of Cr present or with which mineral phases Cr was associated at intermediate to high temperatures. Dehydration and dehydroxylation reactions, occurring in the temperature range between 200 and 400 °C (prior to phase transformation from schwertmannite to hematite) may have favored a slight structural rearrangement within the mineral, which ultimately induced changes in the type of Cr surface complexes. Previous works have reported an increasing contribution of inner-sphere surface complexes with increasing temperature [14,49]. Our results are in agreement with the formation of strongly bound inner-sphere complexes, i.e., As not outcompeting Cr (Figure 6), as well as Fe and Cr showing a congruent dissolution by citrate/ascorbate extraction (Figure 4).

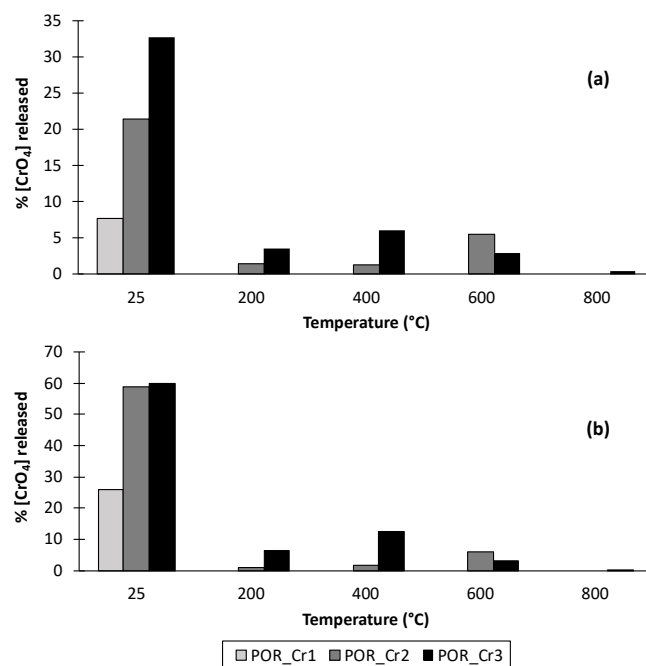


**Figure 6.** CrO<sub>4</sub> released during arsenate adsorption on AMD precipitates and their thermal transformation products at pH 3 and different initial concentrations of arsenate: (a) 170 and (b) 1700 µM.

#### 4. Conclusions

The thermal transformation of iron minerals during wildfires may play an important role in the fate of trace metals. One goal of the present study was to understand the influence of Cr(VI) in the thermal phase transformation of natural AMD-originated schwertmannite to hematite. Another goal was to assess the changes in chromium partitioning upon thermal treatment. These aspects are crucial to understanding the fate of chromium in AMD systems after wildfire events. Our results show that the influence of Cr(VI) on the transformation of schwertmannite to hematite was minimal, as the temperature of transformation, slightly above 600 °C, did not significantly change in the presence of increasing loadings of Cr. However, the mobility of Cr(VI) did undergo a noticeable change after thermal treatment. At room temperature, the mobility of Cr was found to be the highest. As the temperature increased in the range of 25 °C to 400 °C, i.e., temperatures below the transformation to hematite, chromium mobility decreased. The higher the temperature within this range the lower the fraction of exchangeable chromium. For instance, the Cr–As exchange was less likely to occur at higher temperatures, thus contributing to reducing the extent of arsenate adsorption. This phenomenon was attributed to the increased contribution of Cr inner-sphere complexes as temperature increased. At temperatures above 600 °C, chromium became even more stabilized. As a result of the thermal transformation from schwertmannite to hematite a lower surface reactivity was observed, since the adsorption extent of arsenate decreased.

The results presented in this manuscript have implications for the environmental assessment of AMD areas affected by wildfires or any kind of in situ thermal treatment. From the results presented in this study it is evident that although the risk of spreading of other contaminants from AMD may increase due to reduced adsorption behavior of the neo-formed hematite, adsorbed Cr(VI) was stabilized. Moreover, these results could serve as an indication of the long-term stability of AMD in the absence of wildfires, since fast thermal transformation events could result in similar mineralogical transformation to the ones observed upon slow natural aging in dry soil zones. Additional experiments at the microscopic level, such as Cr K-edge EXAFS spectroscopy, would be needed to confirm the mechanistic hypothesis explaining the changes in Cr(VI) binding upon thermal treatment that are discussed in this work.

**Supplementary Materials:** The following supporting information can be downloaded at: <https://www.mdpi.com/article/10.3390/min12060726/s1>, Figure S1: XRD of samples POR<sub>s</sub>, POR\_Cr1, POR\_Cr2, and POR\_Cr3; Figure S2: XRD Cr samples and their thermal transformation products; Figure S3: Changes in the position and FWHM of the XRD peaks upon thermal transformation; Figure S4: FTIR spectra (region 4000 to 2000 cm<sup>-1</sup>) of the POR<sub>s</sub> sample; Table S1: TGA weight loss (%) for AMD samples.

**Author Contributions:** Conceptualization, J.A., A.O.-F. and S.F.; methodology, C.L., J.A, A.O.-F. and S.F.; validation, C.L., A.O.-F. and I.C.; formal analysis, C.L., I.C., P.V.V. and B.D.-M.; investigation, C.L., A.O.-F. and I.C.; resources, J.A. and S.F.; writing—original draft preparation, C.L.; writing—review and editing, J.A., I.C., A.O.-F., P.V.V., B.D.-M. and S.F.; visualization, C.L., A.O.-F. and P.V.V.; supervision, J.A. and S.F.; project administration, S.F.; funding acquisition, J.A. and S.F. All authors have read and agreed to the published version of the manuscript.

**Funding:** This research was funded by the Xunta de Galicia through the Consolidation of competitive groups of investigations program (ED431C 2018/12), and financially supported by the Interreg VA Spain-Portugal Programme (EU) through the project TERRAMATER (0701\_TERRAMATER\_1\_E).

**Data Availability Statement:** Not applicable.

**Acknowledgments:** The authors thank Francisco Casas and María Santiso from the Department of Soil Science and Agricultural Chemistry at USC for their technical assistance in laboratory analysis. The authors would like to extend thanks for the use of the RIAIDT-USC analytical facilities. The authors also thank Felipe Macías García from Centro de Valorización del Norte S.L. for his help with accessing the study site. C.L., J.A. and S.F. belong to the Galician Competitive Research Group (GRC

GI-1245) and to the Cross-disciplinary Research in Environmental Technologies (CRETUS Research Center, ED431E 2018/01). All these programs are co-funded by FEDER (EU).

**Conflicts of Interest:** The authors declare no conflict of interest. The funders had no role in the design of the study; in the collection, analyses, or interpretation of data; in the writing of the manuscript, or in the decision to publish the results.

## References

1. Schoepfer, V.A.; Burton, E.D. Schwertmannite: A review of its occurrence, formation, structure, stability and interactions with oxyanions. *Earth-Sci. Rev.* **2021**, *221*, 103811. [[CrossRef](#)]
2. Bigham, J.M.; Schwertmann, U.; Carlson, L.; Murad, E. A poorly crystallized oxyhydroxysulfate of iron formed by bacterial oxidation of Fe(II) in acid mine waters. *Geochim. Cosmochim. Acta* **1990**, *54*, 2743–2758. [[CrossRef](#)]
3. Bigham, J.M.; Nordstrom, D.K. Iron and aluminium hydroxysulfates from acid sulphate waters. In *Reviews in Mineralogy and Geochemistry—Sulfate Minerals: Crystallography, Geochemistry, and Environmental Significance*; Alpers, C.N., Jambor, J.L., Nordstrom, D.K., Eds.; The Mineralogical Society of America: Washington, DC, USA, 2000; pp. 351–403.
4. Regenspurg, S.; Brand, A.; Peiffer, S. Formation and stability of schwertmannite in acidic mining lakes. *Geochim. Cosmochim. Acta* **2004**, *68*, 1185–1197. [[CrossRef](#)]
5. Antelo, J.; Fiol, S.; Gondar, D.; López, R.; Arce, F. Comparison of arsenate, chromate and molybdate binding on schwertmannite: Surface adsorption vs anion-exchange. *J. Colloid Interface Sci.* **2012**, *386*, 338–343. [[CrossRef](#)]
6. Marouane, B.; Klug, M.; As, K.S.; Enge, J.; Reichel, S.; Janneck, E.; Peiffer, S. The potential of granulated schwertmannite adsorbents to remove oxyanions ( $\text{SeO}_2^{3-}$ ,  $\text{SeO}_2^{4-}$ ,  $\text{MoO}_2^{4-}$ ,  $\text{PO}_3^{4-}$ ,  $\text{Sb}(\text{OH})^{-6}$ ) from contaminated water. *J. Geochem. Explor.* **2021**, *223*, 107708. [[CrossRef](#)]
7. Burton, E.D.; Karimian, N.; Johnston, S.G.; Schoepfer, V.A.; Choppala, G.; Lamb, D. Arsenic-imposed effects on schwertmannite and jarosite formation in acid mine drainage and coupled impacts on arsenic mobility. *ACS Earth Space Chem.* **2021**, *5*, 1418–1435. [[CrossRef](#)]
8. Paikaray, S.; Peiffer, S. Lepidocrocite formation kinetics from schwertmannite in Fe(II)-rich anoxic alkaline medium. *Mine Water Environ.* **2014**, *34*, 213–222. [[CrossRef](#)]
9. Antelo, J.; Fiol, S.; Carabante, I.; Arroyo, A.; Lezama-Pacheco, J.S.; Josevska, N.; Protopapa, C.; Kumpiene, J. Stability of naturally occurring AMD-schwertmannite in the presence of arsenic and reducing agents. *J. Geochem. Explor.* **2021**, *220*, 106677. [[CrossRef](#)]
10. Dhal, B.; Thatoi, H.N.; Das, N.N.; Pandey, B.D. Chemical and microbial remediation of hexavalent chromium from contaminated soil and mining/metallurgical solid waste: A review. *J. Hazard. Mater.* **2013**, *250*, 272–291. [[CrossRef](#)]
11. Xie, J.; Gu, X.; Tong, F.; Zhao, Y.; Tan, Y. Surface complexation modeling of Cr(VI) adsorption at the goethite–water interface. *J. Colloid Interf. Sci.* **2015**, *455*, 55–62. [[CrossRef](#)]
12. Komárek, M.; Koretsky, C.M.; Stephen, K.J.; Alessi, D.S.; Chrástný, V. Competitive adsorption of Cd(II), Cr(VI), and Pb(II) onto nanomaghemite: A spectroscopic and modeling approach. *Environ. Sci. Technol.* **2015**, *49*, 12851–12859. [[CrossRef](#)] [[PubMed](#)]
13. Bompoti, N.M.; Chrysochoou, M.; Machesky, M. A unified surface complexation modeling approach for chromate adsorption on iron oxides. *Environ. Sci. Technol.* **2019**, *53*, 6352–6361. [[CrossRef](#)] [[PubMed](#)]
14. Dabizha, A.; Kersten, M. Exothermic adsorption of chromate by goethite. *Appl. Geochem.* **2020**, *121*, 104785. [[CrossRef](#)]
15. Regenspurg, S.; Peiffer, S. Arsenate and chromate incorporation in schwertmannite. *Appl. Geochem.* **2005**, *20*, 1226–1239. [[CrossRef](#)]
16. Li, X.; Guo, C.; Jin, X.; He, C.; Yao, Q.; Lu, G.; Dang, Z. Mechanisms of Cr(VI) adsorption on schwertmannite under environmental disturbance: Changes in surface complex structures. *J. Haz. Mat.* **2021**, *416*, 125781. [[CrossRef](#)]
17. Fan, C.; Guo, C.; Zeng, Y.; Tu, Z.; Ji, Y.; Reinfelder, J.R.; Chen, M.; Huang, W.; Lu, G.; Yi, X.; et al. The behavior of chromium and arsenic associated with redox transformation of schwertmannite in AMD environment. *Chemosphere* **2019**, *222*, 945–953. [[CrossRef](#)]
18. Choppala, G.; Karimian, N.; Burton, E.D. An X-ray absorption spectroscopic study of the Fe(II)-induced transformation of Cr(VI)-substituted schwertmannite. *J. Haz. Mat.* **2022**, *431*, 128580. [[CrossRef](#)]
19. Johnston, S.G.; Burton, E.D.; Moon, E.M. Arsenic mobilization is enhanced by thermal transformation of schwertmannite. *Environ. Sci. Technol.* **2016**, *50*, 8010–8019. [[CrossRef](#)]
20. Vithana, C.L.; Johnston, S.G.; Dawson, N. Divergent repartitioning of copper, antimony and phosphorus following thermal transformation of schwertmannite and ferrihydrite. *Chem. Geol.* **2018**, *483*, 530–543. [[CrossRef](#)]
21. Das, S.; Hendry, M.J.; Essilfie-Dughan, J. Transformation of two-line ferrihydrite to goethite and hematite as a function of pH and temperature. *Environ. Sci. Technol.* **2012**, *45*, 268–275. [[CrossRef](#)]
22. Grogan, K.L.; Gilkes, R.J.; Lottermoser, B.G. Maghemite formation in burnt plant litter at East Trinity, north Queensland, Australia. *Clays Clay Miner.* **2003**, *51*, 390–396. [[CrossRef](#)]
23. Otero-Fariña, A.; Gago, R.; Antelo, J.; Fiol, S.; Arce, F. Surface complexation modelling of arsenic and copper immobilization by iron oxide precipitates derived from acid mine drainage. *Bol. Soc. Geol. Mex.* **2015**, *67*, 493–508. [[CrossRef](#)]
24. Baleeiro, A.; Fiol, S.; Otero-Fariña, A.; Antelo, J. Surface chemistry of iron oxides formed by neutralization of acidic mine waters: Removal of trace metals. *App. Geochem.* **2018**, *89*, 129–137. [[CrossRef](#)]

25. Álvarez, E.; Fernández-Sanjurjo, M.; Otero, X.L.; Macías, F. Aluminum speciation in the bulk and rhizospheric soil solution of the species colonizing an abandoned copper mine in Galicia (NW Spain). *J. Soil Sediment.* **2011**, *11*, 221–230. [[CrossRef](#)]
26. Asensio, V.; Vega, F.A.; Andrade, M.L.; Covelo, E.F. Tree vegetation and waste amendments to improve the physical condition of copper mine soils. *Chemosphere* **2013**, *90*, 603–610. [[CrossRef](#)] [[PubMed](#)]
27. Burgos, W.D.; Borch, T.; Troyer, L.D.; Luan, F.; Larson, L.N.; Brown, J.F.; Lambson, J.; Shimizu, M. Schwertmannite and Fe oxides formed by biological low-pH Fe(II) oxidation versus abiotic neutralization: Impact on trace metal sequestration. *Geochim. Cosmochim. Acta* **2012**, *76*, 29–44. [[CrossRef](#)]
28. Clesceri, L.S.; Greenberg, A.E.; Eaton, A.D. *Standard Methods for the Examination of Water and Wastewater*, 20th ed.; American Public Health Association: Washington, DC, USA, 1998.
29. Bartlett, R.J.; James, B.R. Chromium. In *Methods of Soils Analysis, Part 3: Chemical Methods*, 1st ed.; Sparks, D.L., Page, A.L., Helmke, P.A., Loeppert, R.H., Soltanpour, P.N., Tabatabai, M.A., Johnston, C.T., Summer, M.E., Eds.; Soil Science Society of America: Madison, WI, USA, 1996; pp. 683–701.
30. Certini, G. Effects of fire on properties of forest soils: A review. *Oecologia* **2005**, *143*, 1–10. [[CrossRef](#)]
31. Blake, D.; Lu, K.; Horwitz, P.; Boyce, M.C. Fire suppression and burnt sediments: Effects on the water chemistry of fire-affected wetlands. *Int. J. Wildland Fire* **2012**, *21*, 557–561. [[CrossRef](#)]
32. Claff, S.R.; Sullivan, L.A.; Burton, E.D.; Bush, R.T. A sequential extraction procedure for acid sulfate soils: Partitioning of iron. *Geoderma* **2010**, *2010* 155, 224–230. [[CrossRef](#)]
33. Keon, N.E.; Swartz, C.H.; Brabander, D.J.; Harvey, C.; Hemond, H.F. Validation of an arsenic sequential extraction method for evaluating mobility in sediments. *Environ. Sci. Technol.* **2001**, *35*, 2778–2784. [[CrossRef](#)]
34. Paul, C.J.; Ford, R.G.; Wilkin, R.T. Assessing the selectivity of extractant solutions for recovering labile arsenic associated with iron (hydr)oxides and sulfides in sediments. *Geoderma* **2009**, *152*, 137–144. [[CrossRef](#)]
35. Lenoble, V.; Deluchat, V.; Serpaud, B.; Bollinger, J.C. Arsenite oxidation and arsenate determination by the molybdene blue method. *Talanta* **2003**, *61*, 267–276. [[CrossRef](#)]
36. Nordstrom, D.K. Mine waters: Acid to circumneutral. *Elements* **2011**, *7*, 393–398. [[CrossRef](#)]
37. Boily, J.F.; Gassman, P.L.; Peretyazhko, T.; Szanyi, J.; Zachara, J.M. FTIR spectral components of schwertmannite. *Environ. Sci. Technol.* **2010**, *44*, 1185–1190. [[CrossRef](#)] [[PubMed](#)]
38. Tresintsi, S.; Simeonidis, K.; Pliatsikas, N.; Vourlias, G.; Patsalas, P.; Mitrakas, M. The role of  $\text{SO}_4^{2-}$  surface distribution in arsenic removal by iron oxy-hydroxides. *J. Solid State Chem.* **2014**, *213*, 145–151. [[CrossRef](#)]
39. Sánchez-España, J.; Yusta, I.; Diez-Ercilla, M. Schwertmannite and hydrobasaluminite: A re-evaluation of their solubility and control on the iron and aluminium concentration in acidic pit lakes. *Appl. Geochem* **2011**, *26*, 1752–1774. [[CrossRef](#)]
40. Caraballo, M.A.; Rimstidt, J.D.; Macías, F.; Nieto, J.M.; Hochella, M.F., Jr. Metastability, nanocrystallinity and pseudo-solid solution effects on the understanding of schwertmannite solubility. *Chem. Geol.* **2013**, *360*, 22–31. [[CrossRef](#)]
41. Sánchez-España, J.; Pamo, E.L.; Santofimia, E.; Aduvire, O.; Reyes, J.; Baretino, D. Acid mine drainage in the Iberian Pyrite Belt (Odiel river watershed, Huelva, SW Spain): Geochemistry, mineralogy and environmental implications. *Appl. Geochem* **2005**, *20*, 1320–1356. [[CrossRef](#)]
42. Antelo, J.; Fiol, S.; Gondar, D.; Pérez, C.; López, R.; Arce, F. Cu(II) incorporation to schwertmannite: Effect on stability and reactivity under AMD conditions. *Geochim. Cosmochim. Acta* **2013**, *119*, 149–163. [[CrossRef](#)]
43. Majzlan, J.; Alpers, C.N.; Kock, C.B.; McCleskey, R.B.; Myneni, S.C.B.; Neil, J.M. Vibrational, X-ray absorption, and Mössbauer spectra of sulfate minerals from the weathered massive sulfide deposit at Iron Mountain, California. *Chem. Geol.* **2011**, *284*, 296–305. [[CrossRef](#)]
44. Pulišová, P.; Máša, B.; Michalková, E.; Večerníková, E.; Maříková, M.; Bezdička, P.; Murafa, N.; Šubrt, J. Thermal behaviour of natural and synthetic iron precipitates from mine drainage. *J. Therm. Anal. Calorim.* **2014**, *116*, 625–632. [[CrossRef](#)]
45. Burton, E.D.; Bush, R.T.; Johnston, S.G.; Watling, K.M.; Hocking, R.K.; Sullivan, L.A.; Parker, G.K. Sorption of arsenic(V) and arsenic(III) to schwertmannite. *Environ. Sci. Technol.* **2009**, *43*, 9202–9207. [[CrossRef](#)] [[PubMed](#)]
46. Cismasu, A.C.; Michel, F.M.; Tcaciuc, A.P.; Tyliczszak, T.; Brown, G.E., Jr. Composition and structural aspects of naturally occurring ferrihydrite. *Compt. Rendus Geosci.* **2011**, *343*, 210–218. [[CrossRef](#)]
47. Yue, P.; Chen, N.; Peak, D.; Bompoti, N.M.; Chrysochoou, M.; Onnis-Hayden, A.; Larese-Casanova, P. Oxygen atom release during selenium oxyanion adsorption on goethite and hematite. *Appl. Geochem.* **2020**, *117*, 104605. [[CrossRef](#)]
48. Waiman, C.V.; Arroyave, J.M.; Chen, H.; Tan, W.; Avena, M.J.; Zanini, G.P. The simultaneous presence of glyphosate and phosphate at the goethite surface as seen by XPS, ATR-FTIR and competitive adsorption isotherms. *Colloid. Surf. A* **2016**, *498*, 121–127. [[CrossRef](#)]
49. Burton, E.D.; Choppala, G.; Vithana, C.L.; Karimina, N.; Hockman, K.; Johnston, S.G. Chromium(VI) formation via heating of Cr(III)-Fe(III)-(oxy)hydroxides: A pathway for fire-induced soil pollution. *Chemosphere* **2019**, *222*, 440–444. [[CrossRef](#)]